Design and testing of slide vibrational compaction device

Chunling Lang[1], Haifeng Qian[1], Zirui Zhu[2], Yanpeng Wei[2], Han Wang[3], Jiale Zhao[2,5*], Jianguang Gong[4,5*]

(1. *College of Mathematics and Computer Engineering, Guangxi Science and Technology Normal University, Laibin 546199, Guangxi, China*;
2. *College of Biological and Agricultural Engineering, Jilin University, Changchun 130025, China*;
3. *College of Mechanical Engineering, Taiyuan University of Technology, Taiyuan 030024, China*;
4. *College Of Computer Science and Technology, Harbin Engineering University, Harbin 150001, China*;
5. *National Key Laboratory of Smart Farm Technologies and Systems, Harbin 150030, China*)

Abstract: In light of the shortcomings in soil compaction observed in ridge cultivation following seeding in Northeast China, it was deemed necessary to develop a solution that would address the issue of soil moisture conservation and temperature control on the seedbed. The slide vibrational compaction device (SVPD), which is capable of compacting the upper and lateral soil of the ridge, was thus designed. The device features adjustable parameters, including an upper compacting plate inlet width of 260-360 mm, an outlet width of 230-290 mm, and a side compacting plate width of 140-240 mm. Its key components include an eccentric block generating vibratory force, a spring system with adjustable stiffness for controlled compaction, and compacting plates designed for uniform soil coverage. The optimal working parameters were determined to be an eccentric block angle of 36.00°, spring stiffness of 46.00 N/mm, and an upper plate exit width of 284.00 mm. The device achieves soil bulk densities of 1.206 g/cm^3 on the ridge and 1.148 g/cm^3 on the ridge side, significantly improving compaction compared to traditional methods, and increasing maize yield by 5%. Therefore, in order to meet the agronomic requirements of soil bulk density for crop growth on the ridge, the sliding vibration compacting device also achieves effective compaction of the soil on the ridge side, providing effective technical support for crop emergence and growth under the monoculture planting pattern in Northeastern China.

Keywords: sliding, vibratory ballast, design and testing, soil bulk density
DOI: 10.25165/j.ijabe.20251803.9140

Citation: Lang C L, Qian H F, Zhu Z R, Wei Y P, Wang H, Zhao J L, et al. Design and testing of slide vibrational compaction device. Int J Agric & Biol Eng, 2025; 18(3): 105–115.

1 Introduction

Soybean, maize, and rice are currently the three main crops grown in Northeastern China, which is an important grain base for the country. Soybean and maize are mostly planted using a monoculture planting mode. After sowing, the soil on the sides of the ridges in monoculture fields is often loose due to a lack of compaction. This loose soil is more susceptible to water and wind erosion[1]. Such erosion not only reduces farmland productivity but also affects air quality[2]. Proper compaction can help mitigate wind erosion[3,4]. Compaction plays a critical role during crop sowing. It increases the seedbed's ability to absorb water by enhancing soil firmness. This ensures close contact between crop seeds and the soil, helping to retain, conserve, and supply moisture[5-10]. Compaction also raises the seedbed's soil temperature, which improves crop emergence rates.

In Northeastern China, spring sowing occurs under challenging conditions. The temperatures are low and dry, with significant day-to-night variations. To address these issues, dry crops are usually planted in ridges. Ridges help reduce soil moisture loss and balance soil temperature. For example, corn is often planted in two or more rows on a ridge[11,12]. In this arrangement, the corn seedbed is located off-center and close to the ridge's side.

After the operation of traditional compaction devices, the soil on the ridge sides remains loose. This loose soil leads to water loss in the soybean seedbed. It is not conducive to moisture conservation and negatively impacts the growth of corn seedlings[13,14]. Loose soil on the ridge side also causes fluctuations in soil temperature at the seedbed. As a result, the average time for crop emergence is prolonged[15].

Domestic and foreign research on compaction devices is relatively scarce[16], and currently the cylindrical compaction roller is the most commonly used device. In the research of compaction devices, Wang et al.[17] designed a variable force seed belt compaction device for precision seeders; Liu et al.[18] designed a multifunctional soil crushing compaction device; Jia et al.[11,12] designed a profiling elastic compaction roller that can solve the problem of longitudinal and transverse profiling; Guo et al.[5] designed a mulching compaction device that can be used for both

Received date: 2024-06-11 **Accepted date:** 2025-02-25
Biographies: **Chunling Lang**, PhD, Assistant Professor, research interest: agricultural machinery and informatization, Computer Vision Email: langchunling2001@126.com; **Haifeng Qian**, Researcher, research interest: agricultural engineering, Email: qianhaifeng2001@126.com; **Zirui Zhu**, Assistant Professor, research interest: agricultural engineering, Email: zrzhu@mails.jlu.edu.cn; **Yanpeng Wei**, PhD, research interest: agricultural machinery and conservation tillage technology, Email: china_dp@163.com; **Han Wang**, PhD, research interest: agricultural machinery and conservation tillage technology, Email: wanghan0405@163.com.
***Corresponding author: Jiale Zhao**, PhD, Professor, research interest: bionic intelligent agricultural machinery and conservation tillage. College of Biological and Agricultural Engineering, Jilin University, Changchun 130025, China. Tel: +86-18843165417, Email: zhaojiale0313@163.com; **Jianguang Gong**, PhD, Professor, research interest: intelligent ploughing machinery. College of Computer Science and Technology, Harbin Engineering University, Harbin 150001, China. Tel: +86-18603650678, Email: gjg@hrbeu.edu.cn.

mulching and compaction; Fukami et al.[19] designed a vibratory smoothing roller that can be used as a vibratory deep loosening machine after smoothing adjustment; and Liu et al.[20] designed a viscosity reduction smoothing device based on the principle of scraping and vibration, which significantly reduces the traction resistance and the amount of soil adhesion. Additionally, Liu et al.[21] designed a bidirectional profiling press device. Field experiments have shown that optimizing the spring deformation of the bidirectional profiling press device can significantly improve crop emergence rate, emergence time, and soil moisture content. All the above compactors have their own advantages, but for post-sowing compaction of monoculture crops in Northeastern China, the above compactors can only be used on the soil on the ridge compaction, but not on the side of the ridge to achieve soil compaction.

In view of the problem of not compacting the soil on the ridge side after sowing in Northeastern China, based on the agronomic pattern and requirements of Northeastern China's monoculture, this paper designs a sliding compacting device with an active vibration function, which ensures that the volume density of the soil on the ridge side meets the agronomic requirements after operation, and at the same time achieves the compacting of the soil on the ridge side, and creates better conditions of warmth and moisture for crop sowing and growth. Soil slot tests were conducted to investigate the effects of eccentric block angle, spring stiffness, and top plate exit width on soil bulk density at the top and side of the ridge and to find the optimum combination of factors. The results of the soil slot tests were verified in the field and compared with the results of the soil slot tests.

2 Vibratory slide compaction device (SVPD)

2.1 Structure and working principle of the whole machine

2.1.1 Whole machine structure

As shown in Figure 1, northeastern corn is usually planted in two or more rows on ridges. Sliding vibratory plate compactors operate to compact ridges prior to planting. Figure 2 shows a schematic diagram of the structure of a sliding vibratory plate compactor, which consists mainly of an upper compaction plate, a lateral compaction plate, a pressure adjusting spring, and a connecting frame. The front end and the rear end of the compactor have a trapezoidal shape in cross section, and the cross-sectional area of the front end is larger than the cross-sectional area of the rear end, so that the adjustment of the width of the compaction plate at the front end and the rear end can be achieved by adjusting the position of the lateral compaction plate during operation. Among them, the adjustable width of the front upper compaction plate is 260-360 mm, the adjustable width of the rear upper compaction plate is 230-290 mm, and the width of the lateral compaction plate can be adjusted to meet the different requirements of the ridge height. The adjustable width of the lateral compaction plate is 140-240 mm, so as to obtain the ridge height of 100-160 mm after the operation.

In the process of operation, the soil from the front end into the sliding vibration compaction device, due to the gradual reduction of cross-sectional area, by the extrusion pressure from the upper compaction plate and the side of the compaction plate, so that the traction force provided by the tractor in the extrusion of the soil on the ridges, and at the same time in the vibration of the vibration motor under the action of the vibration force to achieve the compaction of the ridges, can be adjusted by adjusting the size of the vibration motor eccentric block angle to regulate the size of the vibration force. The size of the vibration force can be adjusted by adjusting the size of the eccentric block of the vibration motor. When the machine is working, the upper compaction plate forms a certain angle U with the top of the ridge; the value of U ranges from 3° to 8°, to prevent the soil above the upper compaction plate from affecting the operation during the working process. At the same time, due to the role of the pressure-regulating spring, the upper pressure plate can always be in contact with the top of the ridge according to the changes in the terrain, so as to better compact the ridge. Different import and export widths can be obtained by adjusting the different mounting positions of the bolts in the oblong holes on the connecting plate and the upper compacting plate, applicable to planting the width of different crops of the monopoly. Adjusting the connecting position of the connecting plate and the side compacting plate to obtain different heights of the monopoly, applicable to planting the height of the monopoly of different crops required.

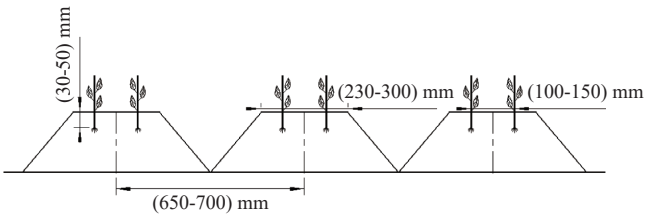

a. Ridge cultivation technique of corn of double row planting pattern

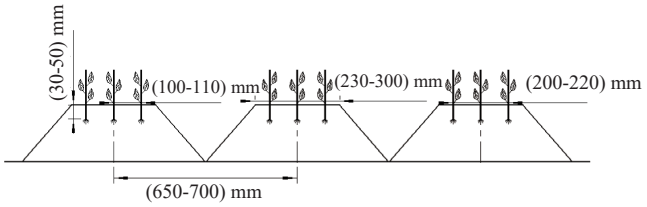

b. Ridge cultivation technique of corn of three row planting pattern

Figure 1 Ridge cultivation technique of corn

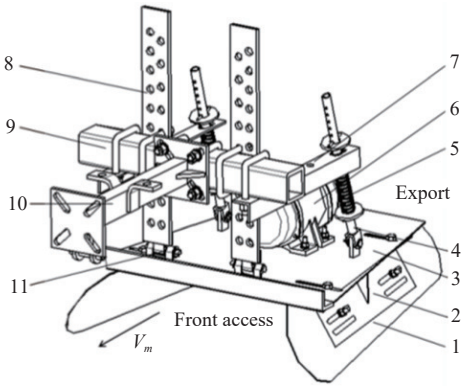

1. Lateral compaction plate 2. Lateral connecting plates 3. Upper compaction plate 4. Pull rod 5. Pressure regulating springs 6. Vibratory motor 7. Upper support 8. Connecting plates 9. Beam 10. Connecting support 11. Hinges

Figure 2 Structure diagram of SVPD

2.1.2 Structural design of the upper compaction plate

According to Figure 3, a sketch of the cross section of the ridge platform after seeding compaction for ridge planting in Northeastern China, it is necessary to determine the width of the upper compaction plate of the compaction device so that the width of the top of the ridge platform after compaction meets the agronomic requirements for ridge planting in Northeastern China. The depth of soil compaction at the top of the row is usually given by the agronomic requirements of the crop to be planted and can be used as raw data for deciding the maximum lateral dimensions of

the top plate of the compaction[22]. It is known from soil mechanics that the pressure in the depth of the soil layer beyond the minimum transverse dimension of the rigid compaction plate decreases sharply during vibratory compaction of the soil. Therefore, the minimum transverse dimension of the ballast plate on the compaction device should be greater than the thickness of the soil layer to be compacted on the mound[23], that is:

$$W_{\min} \geq \delta \tag{1}$$

where, $W_{\min}$ is width of top plate of vibratory compaction device, mm; δ is thickness of soil layer to be compacted on ridges, mm.

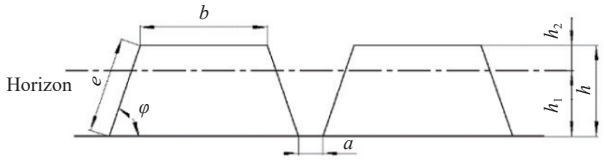

Note: a is width of the furrow of ridge; φ is angle of side; b is width of top surface of ridge platform; h is ridge height; h_1 is tillage depth; h_2 is soil thickness.

Figure 3 Structure diagram of cross section

Practical applications usually take $W_{\min} \geq (1\text{-}2)\delta$, and general crops need a compacted soil layer thickness of 100 mm. Taking into account the compactor in the process of operation, the top of the ridge in the transverse (perpendicular to the direction of the ridge) through the extrusion of the side of the compression plate, the compaction effect on the top of the ridge has an impact, so to determine the upper compression plate effective compression part of the $W_{\min} \geq$ (100-400) mm. However, the width of the top of the ridge in the Northeast region is generally b=230-290 mm, and the maximum width of the effective compaction part of the outlet of the compaction plate in the comprehensive selection is W_{out}=290 mm, and the maximum width at the inlet is W_{in}=360 mm. The length of the upper compaction plate should be determined by the forward speed of the compaction machine and the time required to compact the ridges to the volumetric density of soil required by agronomy[24]:

$$L = \frac{V_m t}{n} \tag{2}$$

where, L is length of the upper plate of the compactor in the direction of the ridge, m; V_m is forward speed of the compactor, m/s; t is time taken to compact ridges to agronomically required bulk density, s; n is number of times required to compact the same area to the agronomically required bulk density.

The effective compaction length L of the upper compaction plate of the compactor must be determined based on the desired soil bulk density, and the upper compaction plate length is usually taken as L=(1-1.15)W[25]. For ease of design, the median dimension W_3 of the trapezoidal top plate is used as the equivalent width to calculate the length L of the top plate, that is:

$$W_3 = \frac{W_{out} + W_{in}}{2} = \frac{290 + 360}{2} = 325 \text{ (mm)} \tag{3}$$

In the design of the upper compaction plate, with the above basis as a reference, one must take into account that the plate is installed at an angle of ε with the top of the ridge, resulting in a reduction in the working length of the plate. This consideration, combined with the agronomic requirements of Northeastern monoculture planting, leads us to take the length of the upper compaction plate as L = 500 mm. Considering the need to install two sides of the compaction plate on both sides of the compaction plate on the compaction device, the initial selection of the compaction width of the short side of the trapezoidal top plate is finally determined to be W_1 = 400 mm, and the width of the long side is determined to be W_2 = 500 mm. As shown in Figure 4, the upper compaction plate features two symmetrically distributed groups of elongated holes. T_1, T_2 points for the upper compaction plate elongated holes and the side of the wrench elongated holes with bolts connected to the intersection of the two points T_1, T_2 dotted line between the two points of the side of the wrench for the position of the position of the adjustment of T_1, T_2 position can be obtained from different on the upper compaction plate inlet and outlet width. The inlet adjustment range is 260-360 mm, and the outlet adjustment range is 230-290 mm. Thus, the size of the trapezoidal shape area of the inlet and outlet can be adjusted.

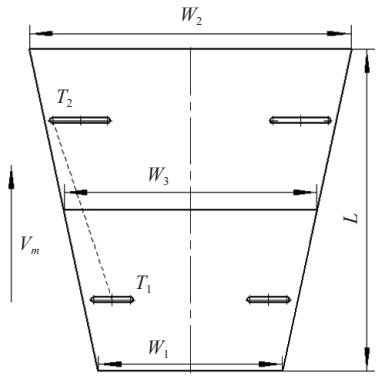

Figure 4 Diagram of upper plate of SVPD

When T_1 and T_2 are in the position shown in Figure 4, assuming that the shape of the compaction inlet and the shape of the outlet (shape of the monopoly table after compaction) are as shown in Figure 5, the ratio of the inlet area S_1 to the outlet area S_2 is defined as the compression ratio δ, that is:

$$\delta = \frac{S_1}{S_2} \tag{4}$$

where,

$$S_1 = \frac{h}{2}\left(b + \frac{2h}{\tan\varphi}\right) \tag{5}$$

$$S_2 = \frac{h'}{2}\left(b' + \frac{2h'}{\tan\varphi'}\right) \tag{6}$$

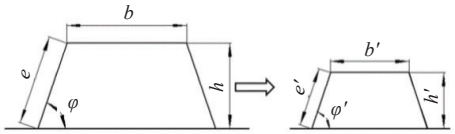

a. Entrance shape b. Exit shape

Figure 5 Structure diagram of entrance and exit of SVPD

Substituting Equations (5) and (6) into Equation (4) gives:

$$\delta = \frac{h\tan\varphi'(b\tan\varphi + 2h)}{h'\tan\varphi(b'\tan\varphi' + 2h')} \tag{7}$$

The compression ratio δ has a greater impact on the compaction effect of the ridge. The larger δ is, the larger the compacted soil bulk density, and the smaller δ is, the smaller the soil bulk density. So, under the condition of meeting the agronomic requirements, the appropriate value of δ should be selected; in this paper, the adjustable range of δ is 1.13-1.56. Provided that b, h, and h' meet the agronomic requirements, it can be seen from Equation (7) that δ can be varied by changing the width of the top plate outlet b' to achieve extrusion of the soil and then using the vibration motor to achieve the appropriate soil bulk density.

2.1.3 Structural design of lateral compaction plate and side connection plate

In Northeastern China, the row height is generally h=100-160 mm, as shown in Figure 3, so first of all it is necessary to determine a reasonable ploughing depth to turn enough soil on the platform to get the appropriate row height. Additionally, to achieve compaction on the side of the rows, it is necessary to determine a reasonable width of the lateral compaction plate according to the required ploughing depth and the height of the platforms.

It is first necessary to determine the depth of ploughing to meet the agronomic requirements. In order to facilitate the calculation, the theoretical assumption is made that the soil in the furrow is all piled up to the platform, the compactor is set forward ds distance, the amount of soil piled up to the platform is dg, the amount of soil turned up from the furrow is also dg, and the theoretical amount of soil in the furrow is:

$$\mathrm{d}G_1 = (ah_1 + h_1^2\cot\varphi)\mathrm{d}s\rho_1 \tag{8}$$

where, ρ_1 is soil bulk density before ploughing, g/cm^3; dG_1 is soil retention volume in furrows under ideal conditions.

However, in practice, the amount of soil piled on the mound is smaller than the theoretical value, so the effective soil turning coefficient λ was introduced, and its value was taken as 0.8-0.9 [14].

$$\mathrm{d}g = \lambda\mathrm{d}G = \lambda(ah_1 + h_1^2\cot\varphi)\mathrm{d}s\rho_1 \tag{9}$$

Assuming negligible subsidence displacement of the soil during compaction, that is, assuming that h_1 does not change after the compactor has worked, the amount of soil piled on top of the mound is:

$$\mathrm{d}G_2 = (bh_2 + h_2^2\cot\varphi)\mathrm{d}s\rho_2 \tag{10}$$

where, ρ_2 is soil bulk density at the top of the ridge after compaction, g/cm^3; dG_2 is soil retention volume on the ridge under ideal conditions.

The following equation can be obtained:

$$\lambda(ah_1 + h_1^2\cot\varphi)\mathrm{d}s\rho_1 = (bh_2 + h_2^2\cot\varphi)\rho_2 \tag{11}$$

Let $\zeta = \dfrac{\rho_2}{\rho_1}$, $h_2 = h - h_1$, then the above equation can be expressed as:

$$\lambda(ah_1 + h_1^2\cot\varphi) - \left[b(h-h_1) + (h-h_1)^2\cot\varphi\right]\zeta = 0 \tag{12}$$

This simplification results in:

$$h_1 = \frac{-a\lambda - \xi(b + 2h\cot\varphi) + \sqrt{\left[a\lambda + \xi(b + 2h\cot\varphi)\right]^2 + 4\zeta\cot\varphi(\lambda - \xi)(bh + h^2\cot\varphi)}}{z(\lambda\cot\varphi - \xi\cot\varphi)} \tag{13}$$

The natural angle of repose of the soil is often 33°-37°. Due to the extrusion of the soil by the compactor, the soil will be gathered to the middle of the ridge, and the inclination of the side of the ridge will be larger after compaction. The angle of inclination of the side of the ridge after compaction is taken as φ=400-430, the width of the top of the ridge as b=230-290 mm, and the width of the ridge groove as a=45-50 mm. The appropriate soil bulk density for crop growth is ρ_2=1.1-1.3 g/cm^3[26,27], and the soil bulk density before ploughing is ρ_1=0.9-1.1 g/cm^3. By selecting the appropriate parameter and substituting it into Equation (13), h_1 can be obtained, which is the determination of the appropriate ploughing depth.

According to the structural sketch of the monopoly platform in Figure 3, the design of the connection structure of the lateral compaction plate and the connecting plate is shown in Figure 5, with the design setting of the inclination angle of the monopoly side after the extrusion of the lateral compaction plate φ =(40°-43°). Then:

$$B = \frac{h}{\sin\varphi} \tag{14}$$

It is taken into account that if the lateral plates come into contact with the grooves during ridge-lateral compaction, this can increase the operating resistance and even damage the lateral plates. At the same time, due to the operation of the upper compaction plate front end and the angle of the ground plane, comprehensive analysis, the shape of the side of the compaction plate will be designed as the front end of the large back end of the two small semicircles, as shown in Figure 5. The large semicircle R_1 = 80 mm, the small semicircle R_2 = 60 mm. Due to the length of the upper compaction plate L = 500 mm, the length of the side of the compaction plate is also taken as 500 mm.

As shown in Figure 6, the side compaction plate can be connected with two groups of elongated holes at different positions of the side plate, which can obtain different widths of the side compaction plate. The adjustable width after connection is 140-240 mm, which can be used to get the height of the ridge to meet the different agronomic requirements after operation. One group of elongated holes on the top of the side plate can be staggered with two groups of elongated holes on the top plate, which can obtain the different widths of the entrance and exit of the pressurizer.

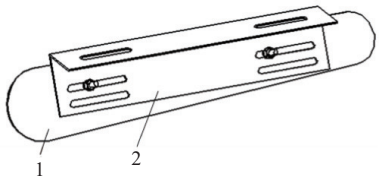

1. Lateral compaction plate 2. Lateral connecting plate

Figure 6 Diagram of connection of lateral plate and connecting plate

2.1.4 Circuit design for compaction device

The wiring diagram of the compactor is shown in Figure 7, including the tractor 12 V power supply, AR-2500 W inverter (power: 2.5 kW, input voltage: 12 V, output voltage: 220 V), WXM-0.4S2-1A frequency converter (power: 1.5 kW, input voltage: single-phase 200 V, output voltage: three-phase 220 V), and YZD-10-2 vibration motor (vibration frequency: 300 r/min). The sliding vibratory compaction device can achieve the compaction of the monopoly by the vibration motor excitation force. This paper selected the YZD-10-2 vibration motor, which has a maximum excitation force of 10 kN. The excitation force can be adjusted by adjusting the vibration motor of the two eccentric block angles. Inverters are not required for the soil bin test, but are required for the field test.

2.2 Force analysis of sliding vibratory compaction device

As shown in Figure 8, the upper compaction plate is subjected to the soil reaction force F_{z3} in the Z direction, the vibration motor eccentric block generated by the Z direction of the force F_{jz}, due to the side of the compaction plate in the left-right symmetrical installation, the X direction of the soil to the size of the reaction force is equal to the direction of the opposite direction, that is F_{x2} = $-F_{x1}$, and at the same time subjected to the eccentric block caused by the horizontal direction of the force F_{jx}, the Z direction of the soil

reaction force F_{z1}, F_{z2} and spring elasticity F_s. Combining the above force analysis and considering that the gravitational force G of the sliding vibration compactor acts on the position of the center of gravity, the force balance equation of the compactor satisfies the following equation:

$$\left.\begin{aligned}\sum F_X &= F_{x1}+F_{x2}+F_{jx}\\ \sum F_Y &= F_{y1}+F_{y2}+F_{sy}\\ \sum F_Z &= F_{z1}+F_{z2}+F_{jz}-G+F_{sz}\end{aligned}\right\} \tag{15}$$

where, F_{jx} and F_{jz} are the components of the excitation force generated by the eccentric block in X and Z directions. F_{jx} and F_{jz} are analyzed:

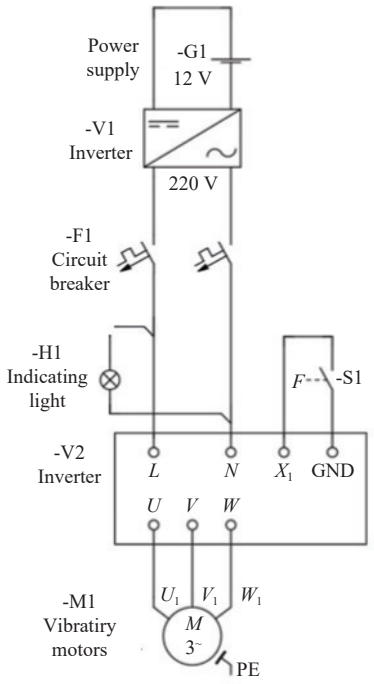

Figure 7 Circuit diagram of SVPD

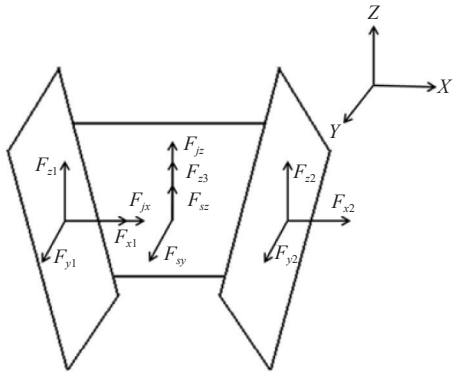

Figure 8 Brief diagram of force analysis of SVPD

The vibration motor spindle is symmetrically installed at each end of the two eccentric blocks; one end is now taken as an example for force analysis. Let the rotational speed of the vibration motor be ω, and the centrifugal forces generated by the two eccentric blocks during rotation be F_{n1} and F_{n2}, respectively:

$$|F_{n1}| = |F_{n2}| = F_n = m\omega^2 r \tag{16}$$

where, m is vibrating motor eccentric mass, g/cm^3; r is eccentric distance, mm; ω is rotation angular velocity, rad/s.

If the installation angle between the two eccentric blocks is $\gamma = \beta - \alpha$, taking the anti-clockwise direction as positive, as shown in Figure 9, then the horizontal components of the centrifugal force generated by the rotation of the two eccentric blocks are F_{x1}, F_{x2}, and the vertical components of the force are F_{z1}, F_{z2}:

$$\left.\begin{aligned}F_{x1} &= F_{N1}\cos(\alpha+\omega t)\\ F_{x2} &= F_{N2}\cos(\beta+\omega t)\end{aligned}\right\} \tag{17}$$

$$\left.\begin{aligned}F_{z1} &= F_{N1}\sin(\alpha+\omega t)\\ F_{z2} &= F_{N2}\sin(\beta+\omega t)\end{aligned}\right\} \tag{18}$$

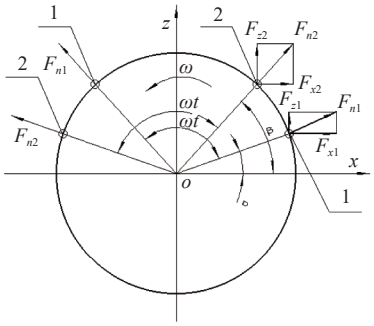

Note: 1 and 2 are the eccentricity blocks; α is initial phase angle of eccentric block 1, (°); β is initial phase angle of eccentric block 2, (°); ω is angular velocity, rad/s; ωt is a turning angle, rad.

Figure 9 Brief diagram of vibrating force analysis

The combined horizontal and vertical forces generated by the centrifugal force of the two eccentric blocks are:

$$F_{jx} = F_{x1}+F_{x2} = F_{N1}\cos(\alpha+\omega t)+F_{N2}\cos(\beta++\omega t) = 2F_N\cos\left(\frac{\alpha+\beta}{2}+\omega t\right)\cos\left(\frac{\alpha-\beta}{2}\right) \tag{19}$$

$$F_{jz} = F_{z1}+F_{z2} = F_{N1}\sin(\alpha+\omega t)+F_{N2}\sin(\beta++\omega t) = 2F_N\sin\left(\frac{\alpha+\beta}{2}+\omega t\right)\sin\left(\frac{\alpha-\beta}{2}\right) \tag{20}$$

The combined force, that is, the excitation force, can be obtained according to the principle of compaction of forces:

$$F = 2F_N\cos\left(\frac{\alpha-\beta}{2}\right) = 2F_N\cos\left(\frac{-\gamma}{2}\right) = 2m\omega^2 r\cos\left(\frac{-\gamma}{2}\right) \tag{21}$$

Orientation: $y = \left(\tan\frac{\alpha+\beta}{2}\right)x$

Therefore, the direction of the combined force F is always on the straight line $y = \left(\tan\frac{\alpha+\beta}{2}\right)x$, and the combined force generated by the two eccentric blocks of the vibration motor at any moment is along the direction of $y = \left(\tan\frac{\alpha+\beta}{2}\right)x$. Changing the initial phase angle of the two eccentric blocks, that is, changing the angle between the two eccentric blocks, can change the magnitude of the component force of the excitation force in the horizontal and vertical directions.

Substituting Equations (19) and (20) into Equation (15), the following equation can be obtained:

$$\left.\begin{aligned}\sum F_X &= 2F_N\cos\left(\frac{\alpha+\beta}{2}+\omega t\right)\cos\left(\frac{\alpha+\beta}{2}\right)\\ \sum F_Y &= F_{y1}+F_{y2}+F_{sy}\\ \sum F_Z &= F_{z1}+F_{z2}+Fz3+\\ 2F_N\sin\left(\frac{\alpha+\beta}{2}+\omega t\right)&\cos\left(\frac{\alpha+\beta}{2}\right)-G+F_{sz}\end{aligned}\right\} \tag{22}$$

As can be seen from Equation (22), the compaction device is mainly subjected to soil reaction force, excitation force, and spring

elasticity. F_{y1}, F_{y2}, F_{z1}, F_{z2} in the case of a certain width of the inlet of the compaction device in the case of the width of the outlet, can be adjusted by adjusting the width of the outlet to change the magnitude of the soil reaction force, the excitation force in the case of a certain m, ω and r, is only associated with the angle between the two eccentric blocks ω, so ω can be regulated to adjust the magnitude of the excitation force. Since the force on the compacting device and the force on the monopoly are action and reaction forces, the pressure on the monopoly can be adjusted by changing the width of the inlet of the compacting device and the size of the angle between the eccentric blocks.

Calculated from Equation (21), the magnitude of the excitation force when γ is at different angles is listed in Table 1.

Table 1 Relationship between angle of eccentric blocks and vibrating force

Angle/(°)	0	60	90	120
Vibrating force/kN	F	0.866F	0.707F	0.5F

3 Soil bin and field test

3.1 Soil bin test

3.1.1 Test method

The test was conducted from 20 to 24 April 2023 at the soil bin test site of the Key Laboratory of Engineering Bionics of the Ministry of Education, Jilin University. The conditions of the soil bin test were as follows: the length of the soil trough was 40 m, the width was 2.8 m, and the depth was 1.8 m. The bulk density of the soil after turning was 1.01 g/cm^3 at a depth of 0-100 mm and 1.24 g/cm^3 at a depth of 100-200 mm. The soil water content was 13.1% at 0-100 mm and 14.9% at 100-200 mm.

During the test, two ridging shovels were attached to the crossbeam of the bin test vehicle and mounted at a distance of 650 mm apart for ridging. The width of the upper compaction plate inlet was adjusted to 330 mm before the test. The soil bin test site is shown in Figure 10a.

a. Soil bin test b. Installation of auxiliary measuring device

Figure 10 Test site in an indoor soil bin

The test equipment included a soil tank trolley test system, a sliding vibratory compaction device, a digital angle ruler, a ridging shovel, an MS-350 moisture meter, a ring-knife assembly with a volume of 100 cm^3 (Hebei Zhongyu Instrument Co., Ltd., China), an electronic scale (LICHEN Instrument Co., Ltd., Zhejiang, China, with an accuracy of 0.01 g), and an auxiliary device for measuring the bulk density of the soil at the side of the ridge. When measuring the bulk density of the soil on the side of the ridge, the auxiliary meter was placed close to the side of the ridge, and the ring knife was inserted into the sleeve to ensure that the direction of the ring knife entering the soil was always perpendicular to the side of the ridge, as shown in Figure 10b.

The soil bin test program was an orthogonal combination test, with each group of tests repeated three times. The average value of the repetitions was taken as the final result for each group. At the end of each test, the bulk density of the soil was measured both above and at the side of the ridge.

3.1.2 Test scheme

The purpose of this soil slot test is to obtain the soil bulk density that meets the agronomic requirements while achieving compaction at the side of the ridge by the orthogonal combination test method, and to investigate the effect of each factor on the soil bulk density above the ridge and at the side of the ridge.

The influencing factors selected for the soil slot test were: eccentric block angle, spring stiffness, and top plate exit width, and three levels were taken for each factor. Based on the Box-Behnken combinational design principle in Design Expert software, this three-factor, three-level orthogonal combinational experiment was designed with 17 trials, including five groups of zero-point trials, using soil bulk density above and at the side of the ridge as the experimental index. The factor level codes are given in Table 2.

Table 2 Experimental factors and levels

Level	Factor		
	Angle of eccentric block/(°)	Spring stiffness/ N·mm^{-1}	Upper plate exit width/mm
–1	0	30	260
0	60	40	275
1	120	50	290

3.1.3 Soil bin test result

This soil bin test was conducted with the level coded values of each factor as the independent variables and the soil bulk density at the top and side of the ridge as the test indices. x_1, x_2, and x_3 are the factor coded values of the eccentric block angle, spring stiffness, and upper plate exit width, respectively, and the test program and results are listed in Table 3.

Table 3 Test scheme and results

Test number	x_1	x_2	x_3	Ridge soil bulk density/g·cm^{-3}	Ridge side soil bulk density/g·cm^{-3}
1	–1	–1	0	1.19	1.16
2	1	–1	0	1.11	1.04
3	–1	1	0	1.18	1.03
4	1	1	0	1.01	1.02
5	–1	0	–1	1.27	1.21
6	1	0	–1	1.18	1.18
7	–1	0	1	1.16	1.16
8	1	0	1	1.08	0.99
9	0	–1	–1	1.19	1.21
10	0	1	–1	1.21	1.12
11	0	–1	1	1.13	1.08
12	0	1	1	1.07	1.01
13	0	0	0	1.27	1.26
14	0	0	0	1.26	1.24
15	0	0	0	1.25	1.22
16	0	0	0	1.24	1.25
17	0	0	0	1.25	1.23

3.1.4 Analysis of variance (ANOVA) of soil bin test results

After processing the data using Design-Expert software, the results of the ANOVA for soil bulk density on ridges were obtained as shown in Table 4. Quadratic multiple regression was fitted to the data in Table 4 to obtain the quadratic multiple regression equation of soil bulk density on coded independent variables on monopoly as:

$$y_1 = 1.25 - 0.052x_1 - 0.019x_2 - 0.051x_3 - 0.023x_1x_2 - 0.020x_2x_3 - 0.055x_1^2 - 0.077x_2^2 - 0.027x_3^2 \quad (23)$$

Table 4 Variance analysis of soil bulk density on top of ridge

Source of variance	Sum of square	Degree of freedom	Mean square	F value	p-value
Model	0.094	9	0.010	37.57	<0.0001
x_1	0.022	1	0.022	79.36	<0.0001
x_2	2.812×10^{-3}	1	2.812×10^{-3}	10.12	0.0155
x_3	0.021	1	0.021	75.62	<0.0001
x_1x_2	2.025×10^{-3}	1	2.025×10^{-3}	7.29	0.0307
x_1x_3	2.500×10^{-5}	1	2.500×10^{-5}	0.090	0.7729
x_2x_3	1.600×10^{-3}	1	1.600×10^{-3}	5.76	0.0475
x_1^2	0.013	1	0.013	45.01	0.0003
x_2^2	0.025	1	0.025	89.85	<0.0001
x_3^2	3.069×10^{-3}	1	3.069×10^{-3}	11.05	0.0127
Lack of fit	1.425×10^{-3}	3	4.750×10^{-4}	3.40	0.1214
Pure error	5.200×10^{-4}	4	1.300×10^{-4}	—	—
Sum	0.096	16	—	—	—

According to the ANOVA results in Table 4, it can be seen that the influence factors x_1, x_2, x_3, x_1x_2, x_2x_3, x_1^2, x_2^2, and x_3^2 are highly significant, and the other influence factors are not significant. The p-value of the out-of-fit term is 0.1214, and it is obvious that p>0.05, indicating that the quadratic multivariate regression has a high degree of fit and there are no out-of-fit factors, so the equation can be used instead of the real test point for analysis. The importance of each factor on the volumetric density of the soil above the ridge can also be obtained, in descending order of importance: the eccentric block angle, the width of the outlet of the top plate, and the stiffness of the spring.

After processing the data using Design-Expert software, the ANOVA results for soil bulk density on the side of the ridge were obtained as listed in Table 5. Quadratic multiple regression was fitted to the data in Table 5 to obtain the quadratic multiple regression equation for soil bulk density on the side of the ridge on the coded independent variables as:

$$y_2 = 1.24 - 0.039x_1 - 0.034x_2 - 0.090x_3 - 0.023x_1x_2 - 0.089x_1^2 - 0.084x_2^2 - 0.026x_3^2 \quad (24)$$

Table 5 Variance analysis of soil bulk density on side of ridge

Source of variance	Sum of square	Degree of freedom	Mean square	F	p
Model	0.16	9	0.018	121.13	<0.0001
x_1	0.012	1	0.012	82.04	<0.0001
x_2	9.113×10^{-3}	1	9.113×10^{-3}	62.23	<0.0001
x_3	0.065	1	0.065	442.54	<0.0001
x_1x_2	2.025×10^{-3}	1	2.025×10^{-3}	13.83	0.0075
x_1x_3	1.000×10^{-4}	1	1.000×10^{-4}	0.68	0.4358
x_2x_3	1.000×10^{-4}	1	1.000×10^{-4}	0.68	0.4358
x_1^2	0.033	1	0.033	226.49	<0.0001
x_2^2	0.030	1	0.030	201.69	<0.0001
x_3^2	2.901×10^{-3}	1	2.901×10^{-3}	19.81	0.0030
Lack of fit	2.500×10^{-5}	3	8.333×10^{-6}	0.033	0.9906
Pure error	1.000×10^{-3}	4	2.500×10^{-4}	—	—
Sum	0.16	16	—	—	—

According to the ANOVA results in Table 5, it can be seen that the influence factors x_1, x_2, x_3, x_1x_2, x_1^2, x_2^2, and x_3^2 are highly significant, and the other influence factors are not significant. The p-value of the out-of-fit term is 0.9906, and it is obvious that p>0.05, which indicates that the quadratic multivariate regression has a high degree of fit, and there is no presence of out-of-fit factors, so the equation can be used instead of the experimental real point for analysis. It can also be seen that the importance of each influencing factor on the volume density of the soil above the ridge is, in descending order of importance, the width of the outlet of the upper plate, the eccentric block angle, and the stiffness of the spring.

3.1.5 Response surface method analysis of soil bin test results

Response surface analysis in Design-Expert software was used to analyze the effects of three influencing factors, namely eccentric block angle, spring stiffness, and top plate outlet width, on the bulk density of the soil above the ridge and the side edges. One of the three factors was set to zero in the analysis, and the effects of the other two factors on the bulk density of the soil above the ridge and on the side edges were investigated.

(1) Effect of eccentric block angle and spring stiffness on bulk density of soil above the ridge

If the width of the outlet of the top plate is fixed at 275 mm, the relationship between the eccentric block angle and the stiffness of the spring on the volumetric density of the soil on the ridge can be obtained as follows:

$$y_1 = 1.25 - 0.052x_1 - 0.019x_2 - 0.023x_1x_2 - 0.055x_1^2 - 0.077x_2^2 \quad (25)$$

From Figure 11 and Equation (25), it can be seen that under the test condition that the width of the outlet of the upper plate is 275 mm, the effect of the eccentric block angle on the volume density of the soil above the ridge is more significant than that of the spring stiffness. The volume density of the soil above the ridge first increases and then decreases with the increase of the spring stiffness; the volume density of soil above the ridge first increases and then decreases with the increase of the eccentric block angle, with a greater trend of change; and the eccentric block angle and the spring stiffness have interactive effects on the volume density of soil above the ridge. Soil bulk density on the ridge, eccentric block angle, and spring stiffness have interactive effects on soil bulk density above the ridge.

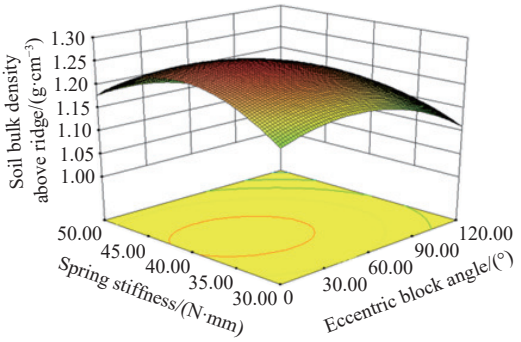

Figure 11 Response surface showing effects of eccentric block angle and spring stiffness on soil bulk density above ridge

(2) Effect of eccentric block angle and top plate exit width on bulk density of soil above the ridge

The fixed spring stiffness is 40 N/mm, and the relationship between the eccentric block angle and the width of the upper plate inlet on the volume density of the soil above the ridge can be obtained as:

$$y_1 = 1.25 - 0.052x_1 - 0.051x_2 - 0.055x_1^2 - 0.027x_3^2 \quad (26)$$

From Figure 12 and Equation (26), it can be seen that under the test condition of spring stiffness of 40 N/mm, the effect of eccentric block angle on the bulk density of soil above the ridge is more significant than that of the width of the upper plate outlet. The bulk density of soil above the ridge increases with the increase of eccentric block angle, and then decreases with a larger change; the bulk density of soil above the ridge increases with the decrease of the width of the upper plate outlet. There is no interaction effect between the eccentric block angle and the width of the upper plate outlet on the bulk density of soil; there is no interaction effect between the eccentric block angle and the width of the upper plate outlet on the bulk density of the soil at the ridge; and there is no interaction effect between the eccentric block angle and the width of the upper plate outlet on the bulk density of the soil at the ridge.

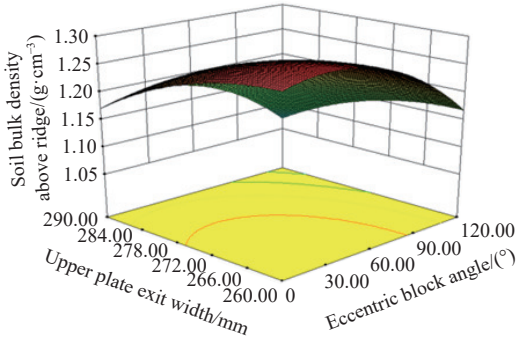

Figure 12 Response surface showing effects of eccentric block angle and upper plate exit width on soil bulk density above ridge

(3) Influence of spring stiffness and upper plate exit width on soil bulk density above the ridge

Fixing the eccentric block angle at 60°, the relationship between the spring stiffness and the width of the upper plate outlet on the volume density of the soil above the ridge can be obtained as:

$$y_1 = 1.25 - 0.019x_2 - 0.051x_3 - 0.020x_2x_3 - 0.077x_2^2 - 0.027x_3^2 \quad (27)$$

From Figure 13 and Equation (27), it can be seen that under the test conditions of 60° eccentric block angle, the effect of the upper plate exit width on the soil bulk density above the ridge is more significant than that of the spring stiffness. The soil bulk density above the ridge tends to increase with the decrease of the upper plate exit width, and the magnitude of the change is larger; the soil bulk density above the ridge tends to first increase and then decrease with the increase of the spring stiffness, and the magnitude of the change is smaller. The spring stiffness and the width of the upper plate exit have an interactive effect on the soil bulk density above the ridge.

(4) Effect of eccentric block angle and spring stiffness on soil volumetric density on the side of the ridge

If the exit width of the top plate is fixed at 275 mm, the relationship between the eccentric block angle and the spring stiffness on the bulk density of the soil on the ridge side can be obtained as follows:

$$y_2 = 1.24 - 0.039x_1 - 0.034x_2 - 0.023x_1x_2 - 0.089x_1^2 - 0.084x_2^2 \quad (28)$$

From Figure 14 and Equation (28), it can be seen that under the test conditions of 275 mm width of the upper plate outlet, the effect of eccentric block angle on the soil bulk density on the side of the ridge is more significant than that of spring stiffness; the soil bulk density on the side of the ridge increases and then decreases with the increase of spring stiffness, and the magnitude of the change is larger. The interaction effect between eccentric block angle and spring stiffness on ridge side bulk density is significant; the effect of eccentric block angle on ridge side bulk density is more significant than that of spring stiffness. There was an interaction effect between eccentric block angle and spring stiffness on the bulk density on the side of the ridge.

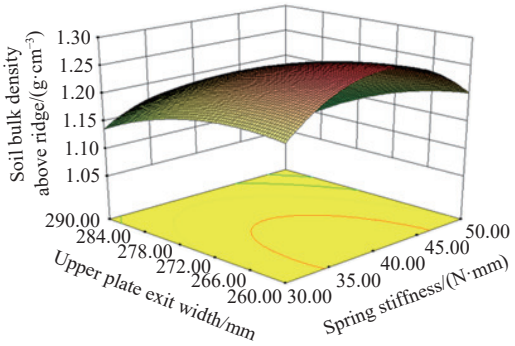

Figure 13 Response surface showing effects of spring stiffness and upper plate exit width on soil bulk density above ridge

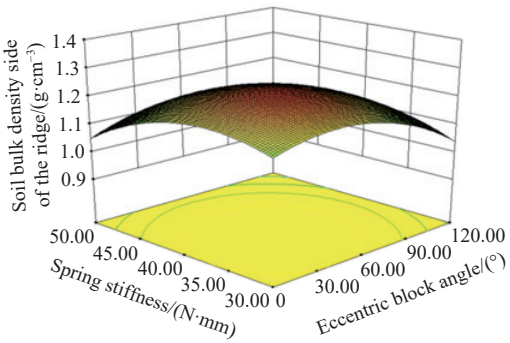

Figure 14 Response surface showing effects of eccentric block angle and spring stiffness on soil bulk density on side of ridge

(5) Effect of eccentric block angle and top plate exit width on soil bulk density on the side of the ridge

The fixed spring stiffness is 40 N/mm, and the relationship between the eccentric block angle and the width of the top plate outlet to the bulk density of the soil on the ridge side can be obtained as follows:

$$y_2 = 1.24 - 0.039x_1 - 0.090x_3 - 0.089x_1^2 - 0.026x_3^2 \quad (29)$$

From Figure 15 and Equation (29), it can be seen that under the test condition of the spring stiffness of 40 N/mm, the effect of the upper plate exit width on the soil bulk density on the ridge side is more significant than that of the eccentric block angle. The soil bulk density on the ridge side increases and then decreases with the increase of the eccentric block angle, and the magnitude of the change is small. The soil bulk density on the side of the ridge increases with the decrease of the upper plate exit width, and the magnitude of the change is large. The eccentric block angle and the upper plate exit width have no interaction effect on the soil bulk density on the side of the ridge; the upper plate exit angle has no effect on the soil bulk density on the side of the ridge. There was no interaction between the eccentric block angle and the width of the top plate outlet on the ridge side bulk density.

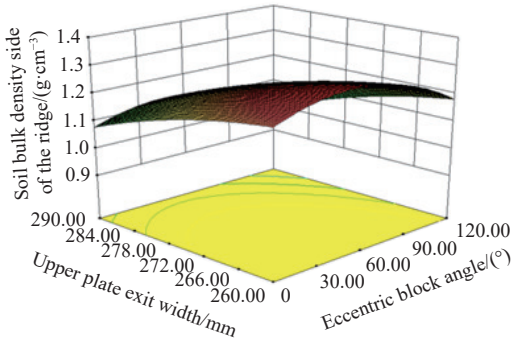

Figure 15 Response surface showing effects of eccentric block angle and upper plate exit width on soil bulk density on side of ridge

(6) Effect of spring stiffness and upper plate exit width on soil bulk density on the side of the ridge

If the eccentric block angle is fixed at 60°, the relationship between the spring stiffness and the width of the upper plate outlet to the bulk density of the soil on the side of the ridge can be obtained as follows:

$$y_2 = 1.24 - 0.034x_2 - 0.090x_3 - 0.089x_1^2 - 0.026x_3^2 \quad (30)$$

From Figure 16 and Equation (30), it can be seen that under the test conditions of 60° eccentric block angle, the effect of the upper plate exit width on the soil bulk density on the ridge side is more significant than that of the spring stiffness. The soil bulk density on the ridge side tends to increase with the decrease of the upper plate exit width, and the magnitude of the change is larger. The soil bulk density on the side of the ridge tends to first increase and then decrease with the increase of the spring stiffness, and the magnitude of the change is smaller. The spring stiffness and the width of the upper plate exit had no interaction effect on the soil bulk density on the side of the ridge.

Based on experimental regression design and fitting, further optimization using Design Expert software predicted the optimum combination of operating parameters to meet the soil bulk density requirements for crop growth as: eccentric block angle 36.00°, spring stiffness 46.00 N/mm, and top plate outlet width 284.00 mm.

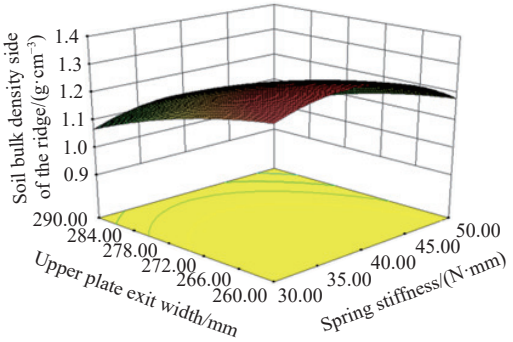

Figure 16 Response surface showing effects of spring stiffness and upper plate exit width on soil bulk density on side of ridge

3.2 Field test

3.2.1 Test method

The experiment was conducted at the experimental field of Jilin Academy of Agricultural Machinery Science from 2 to 5 May 2023, and comparative and field validation tests were conducted. The physical characteristics of the soil in the experimental field were as follows: the tillage method was ridge and furrow, the soil moisture content after tillage was 10.9% for 0-100 mm and 14.2% for 100-200 mm, and the soil bulk density was 1.02 g/cm^3 for soil depths of 0-100 mm and 1.18 g/cm^3 for soil depths of 100-200 mm. The test field was a maize field without stubble cover, and the omni-directional compaction device was connected to a 2BYMQF-4 maize planter towed by a John Deere 904 tractor. The test field is shown in Figure 17.

Main test instruments and equipment: Sliding vibratory compactor, John Deere 904 tractor, 2BYMQF-4 planter, ring knife assembly (Hebei Zhongyu Instrument Co., Ltd., China, with a volume of 100 cm^3), electronic digital scales (LICHEN Instrument Co., Ltd., Zhejiang, China, with an accuracy of 0.01 g), digital display angle ruler (SYNTEK GmbH, Germany, with a resolution of 0.05°).

a. Installation site of SVPD b. Test site c. Comparative compaction device d. Partial enlarged detail

Figure 17 Test site of sowing in the field

The field test was a validation and comparison test in which the machine's operating speed was set to 1 m/s, the machine was operated for 100 m to measure a set of data, and each set of measurements was repeated 10 times.

3.2.2 Field test results

The purpose of the field test was to verify whether the main working parameters obtained from the soil bin test to achieve the soil bulk density required for crop growth had good working results and good effect on crop yield. The verification test was conducted using a 2BYMQF-4 planter developed by Jilin University, and the test was conducted at the Jilin Agricultural Machinery Scientific Research Institute with 10 replications to eliminate random errors during the test.

Sliding vibratory compaction device and the traditional cylindrical compaction roller were both used in the operation of each of the 10 rows to test the compaction effect. Five measurement points were randomly selected on each of the selected rows on the ridge and the side of the ridge, and the average values of the soil bulk density of the ridge and on the side of the ridge over a total of 10 groups of tests were taken. The bulk density of the soil after compaction is listed in Table 6, and the results of the operation test are: the average value of the bulk density of the soil on the ridge

after the operation of the sliding vibratory compaction device is 1.206 g/cm^3; the average value of the bulk density of the soil on the ridge after the operation of the traditional cylindrical compaction roller is 1.188 g/cm^3; and the average value of the bulk density of the soil on the ridge after the operation of the sliding vibratory compaction device is 1.148 g/cm^3, and the average value of soil bulk density on the ridge side after the operation of the sliding vibratory compactor is 1.148 g/cm^3, and the average value of soil bulk density on the ridge side after the operation of the sliding vibratory compactor is 0.971 g/cm^3. The average value of soil bulk density on the uncompacted side of the ridge is 0.971 g/cm^3. The most suitable soil bulk density for crop cultivation is generally 1.0-1.3 g/cm^3[25]. From the experimental results, it can be seen that the sliding vibratory compaction device and the traditional cylindrical compaction rollers can meet the agronomic requirements of crop growth. The sliding vibratory compaction device after the operation of the ridge soil bulk density relative to the traditional cylindrical compaction rollers increased by 1.49%, but the sliding vibratory compaction device to meet the ridge soil bulk density, also achieve the compression of the soil on the side of the ridge, the soil bulk density of the side of the ridge increased by 18.2% relative to the conventional cylindrical compaction roller, making the soil bulk density of the side of the ridge relative to the conventional cylindrical compaction roller increased by 18.2%, making the soil bulk density of the side of the ridge relative to the traditional cylindrical compaction rollers. However, the sliding vibration compaction device in meeting the volume density of soil on the ridge, but also achieved the compaction of soil on the side of the ridge. The soil volume density on the side of the ridge was increased by 18.2% relative to the traditional cylindrical compaction roller, so that the soil volume density on the side of the ridge relative to the uncompacted soil has been significantly improved.

Table 6 Soil bulk density after compaction g/cm^3

Test No.	Vibratory slide compaction device		Conventional cylindrical compaction roller	
	Above the ridge	Side of ridge	Above the ridge	Side of ridge
1	1.18	1.23	1.18	0.92
2	1.22	1.12	1.22	0.96
3	1.16	1.11	1.19	1.01
4	1.25	1.08	1.26	1.03
5	1.23	1.18	1.08	0.94
6	1.21	1.08	1.27	1.03
7	1.18	1.09	1.21	0.92
8	1.25	1.19	1.06	1.03
9	1.20	1.19	1.18	0.95
10	1.18	1.24	1.23	0.92
Average value	1.206	1.148	1.188	0.971

The maize quality measurement test was conducted on 9-10 October 2023 in the experimental field of Jilin Agricultural Machinery Scientific Research Institute, with the aim of verifying the effect on maize yield after the operation of sliding vibratory compaction device. In order to eliminate random error in the test process, the maize planting areas after the operation of different compaction devices were randomly selected, and the measurements were repeated three times in each area. The area was selected to be 8 m long and 0.65 m wide, with a total area of 5.2 m^2, and 10 different areas were selected for 10 replications. The harvested field trial area is shown in Figure 18, and the statistical data are listed in Table 7.

a. Artificial harvest b. Measurement of ear length c. Weighing site

Figure 18 Test site of harvesting in the field

Table 7 Maize yield and its components

Type of compaction device	Maize ear length/ cm	Row number/ row	Maize grain number/ grain	Maize 100-seed weight/g	Yield/ kg·hm^{-2}
Vibratory slide compaction device	21-23	14-16	450-550	32-35	10 500-11 000
Conventional cylindrical compaction roller	20-22	14-16	430-500	31-33	10 000-10 500

4 Conclusions

(1) Based on the agronomic characteristics of ridge planting in Northeastern China, a sliding vibratory compaction device suitable for post-sowing compaction of ridge planting was designed to realize compaction of soil above the ridge and on the side of the ridge.

(2) By the three-factor, three-level orthogonal combination test, Design Expert software was used to analyze the significance of the factors on the soil bulk density above the ridge in the following order: eccentric block angle, the width of the upper plate outlet, and the spring stiffness. The significance of the factors on the soil bulk density on the side of the ridge were analyzed in the following order: the width of the upper plate outlet, the eccentric block angle, and the spring stiffness.

(3) The optimum combination of working parameters to meet the soil bulk density requirements for crop growth was analyzed by the Design Expert software as follows: eccentric block angle of 36.00°, spring stiffness of 46.00 N/mm, and top plate outlet width of 284.00 mm. The validation test and comparison test were carried out, yielding the following results: the average value of soil bulk density on the ridge after the operation of the sliding vibratory compaction device was 1.206 g/cm^3, the average value of soil bulk density on the ridge after the operation of the conventional cylindrical compaction roller was 1.188 g/cm^3, the average value of soil bulk density on the ridge after the operation of the sliding vibratory compaction device was 1.148 g/cm^3, and the average value of soil bulk density on the ridge after the operation of the conventional cylindrical compaction roller was 1.148 g/cm^3. After the operation of the sliding vibratory compactor, the volume density of the soil above and to the side of the ridge increased by 1.49% and 18.2%, respectively, compared to that of the conventional cylindrical compaction roller, which achieved compaction of the soil to the side of the ridge and resulted in a significant increase in the volume density of the soil to the side of the ridge compared to that of the uncompacted soil. After carrying out maize yield measurements, it was found that the maize yield after operation of the sliding vibratory compactor was 5% higher than that of the conventional cylindrical compaction roller.

In this study, a vibration motor was used to provide the excitation force, which may have affected the tractor battery. In the subsequent experimental study, it will be considered to change it to mechanical input power to generate vibration.

Acknowledgements

We acknowledge that this research was financially supported by the National Key Research and Development Program of China (Grant No. 2024YFD2000100), Science and Technology Development Plan Project of Jilin Province (20240303037NC), Project of Education Department of Jilin Province (JJKH20241313HT), Intelligent Control System of Variable Fertilization of Deep Application Liquid Fertilizer (GXKS2022GKY003), and Key Laboratory of Detection Technology for Sugarcane and Peanut Leaf Spot Disease at Guangxi Science and Technology Normal University (GXKSKYPT2025008).

[References]

[1] Yang X, Guo J F, Liu H H, Liu B Y. Soil wind erosion environment in black soil region in Northeastern China. Scientia Geographica Sinica, 2006; 4: 4443–4448.

[2] Zhou Q Q. Numerical simulation on soil wind-blown erosion from cropland in northeastern China. Northeast Institute of Geography and Agricultural Ecology, Chinese Academy of Sciences, 2014. (in Chinese)

[3] Jia H L, Ma C L, Tong J. Study on universal blade rotor for rototilling and stubble-breaking machine. Soil & Tillage Research, 2007; 94(1) 201–208.

[4] Jia H L, Ma C L, Liu Z C, Yang Q, Li G Y, Liu H. Overview of study on the tillage mode of water storage and soil moisture conservation for dry farming region in Northern China. Transactions of the CSAM, 2007; 12: 190–194, 207. (in Chinese)

[5] Guo H, Chen Z, Jia H L, Zheng T Z, Wang G, Wang Q. Design and experiment of soil-covering and soil-compacting device with cone-shaped structure of wheel. Transactions of the CSAE, 2017; 33(12): 56–65. (in Chinese)

[6] Wu J, Tang Q, Yuan W S, Wang S F, Wu C Y. Design and parameter optimization of ditching and compacting parts of rapeseed carpet seedling transplanter. Transactions of the CSAE, 2016; 32(21): 46–53. (in Chinese)

[7] Jia H L, Guo H, Guo M Z, Wang L C, Zhao J L, Fan X H. Finite element analysis of performance on elastic press wheel of row sowing plow machine for covering with soil and its experiment. Transactions of the CSAE, 2015; 31(21): 9–16. (in Chinese)

[8] Tong J, Zhang Z H, Chen D H, Zhang Q Z, Ma Y H. Three-dimensional dynamic finite element analysis of interaction between toothed wheel and soil. Transactions of the CSAE, 2014; 30(10): 48–58. (in Chinese)

[9] Zhang Z H, Tong J, Chen D H, Sun J Y, Ma Y H. Modal analysis of bionic convex teeth rolling component composed of different materials. Transactions of the CSAE, 2012; 28(13): 8–15. (in Chinese)

[10] Zhao J L, Zhang C L, Wei Y P, Guo M Z, Chen C, Zhang C Q, et al. Design and testing of planting unit for rice dry-direct-seeding planter in cold region. Int J Agric & Biol Eng, 2023; 16(4): 76–84.

[11] Wang W J. Bionic press device with profiling mechanism for soybean precision planter. Changchun: Jilin University, 2016. (in Chinese)

[12] Jia H L, Wang W J, Zhuang J, Luo X F, Yao P F, Li Y. Design and experiment of profiling elastic press roller. Transactions of the CSAM, 2015; 46(6): 28–34, 83. (in Chinese)

[13] Zhao J L, Lu Y, Wang X G, Zhuang J, Han Z W. A bionic profiling-energy storage device based on MBD-DEM coupled simulation optimization reducing the energy consumption of deep loosening. Soil & Tillage Research, 2023; 234: 105824.

[14] Voorhees W B, Evans S D, Warnes D D. Effect of preplant wheel traffic on soil compaction, water use, and growth of spring wheat. Soil Sci. Soc. Am. J, 1985; 49(1): 215–220.

[15] Ma S Q, Wang Q, Lv H Q, Xv L P, Yu H, Zhang T L. Impact of water and temperature on spring maize emergence speed and emergence rate. Acta Ecologica Sinica, 2012; 32(11): 3378–3385.

[16] Wu P T, Feng H. Discussion of the development strategy of water saving agriculture in China. Transactions of the CSAE, 2005; 21(6): 152–157. (in Chinese)

[17] Wang J L, Ma X, Lu B, Xv J. Experimental study on seeding strip press roller with variable pressure of precision planter. Journal of Jilin Agricultural University, 2009; 31(4): 472–475. (in Chinese)

[18] Tang Q, Wu C Y, Yuan W S, Wu J, Wang S F. Structure design on compacting and covering soil device of rape shallow transplanting machine. Journal of Chinese Agriculture Mechanization, 2016; 37(3): 20–22. (in Chinese)

[19] Fukami K, Mukunoki T, Nakano K, Matsuo N, Okayasu T. Water leakage control by using vibratory roller on a dry-seeded rice field in southwestern Japan. Soil & Tillage Research, 2017; 166: 138–146.

[20] Liu H J, Zhao S H, Tan H W, Yang Y Q, Zhang X M. Investigation on press device in reducing adhesion and resistance based on scrape and vibration principle. Transactions of the CSAM, 2018; 49(1): 86–92. (in Chinese)

[21] Liu H J, Zhang W Y. Working performance of bidirectional profiling press device in hilly areas of northeast China. Agriculture, 2022; 12(9): 1365.

[22] Cao Z Y, Liu Y L, Wu W R, Tang C M, Yuan W J. Study of the hydraulic vibrator about plate vibrator. Modern Manufacturing Engineering, 2009; 3: 109–111. (in Chinese)

[23] Wang Z Q. Study and practise of plate vibratory compactor. Shijiazhuang: Hebei University of Technology. 2002. (in Chinese)

[24] Yang W C, He J, Lu C Y, Lin H, Yang H Y, Li H. Current situation and future development direction of soil covering and compacting technology under precision seeding conditions in China. Applied Sciences, 2023; 13(11): 6586.

[25] Ren L D, Wang L, Lin L, Zhang B. The progress and prospect of soil compaction by agricultural machinery in arable land: A Review. Acta Pedologica Sinica, 2023; 60(3): 610–626.

[26] Liu M Y, Cai H, Hu C L, Xie B L. Simulation analysis and experiment of eccentric vibration compaction ridge building machine. Journal of Agricultural Mechanization Research, 2023; 45(2): 21–28. (in Chinese)

[27] Fu Q K, Jian S C, Jia H L, Zhao W G, Lv A M, Wei G J. Design and experiment on maize stubble cleaning fertilization ridging seeder. Transactions of the CSAE, 2016; 32(4): 9–16. (in Chinese)